LETTER

https://doi.org/10.1038/s41586-019-0939-3

Recalibration of path integration in hippocampal place cells

Ravikrishnan P. Jayakumar[1,6], Manu S. Madhav[2,6]*, Francesco Savelli[2], Hugh T. Blair[3], Noah J. Cowan[1,4,7] & James J. Knierim[2,5,7]

Hippocampal place cells are spatially tuned neurons that serve as elements of a 'cognitive map' in the mammalian brain[1]. To detect the animal's location, place cells are thought to rely upon two interacting mechanisms: sensing the position of the animal relative to familiar landmarks[2,3] and measuring the distance and direction that the animal has travelled from previously occupied locations[4–7]. The latter mechanism—known as path integration—requires a finely tuned gain factor that relates the animal's self-movement to the updating of position on the internal cognitive map, as well as external landmarks to correct the positional error that accumulates[8,9]. Models of hippocampal place cells and entorhinal grid cells based on path integration treat the path-integration gain as a constant[9–14], but behavioural evidence in humans suggests that the gain is modifiable[15]. Here we show, using physiological evidence from rat hippocampal place cells, that the path-integration gain is a highly plastic variable that can be altered by persistent conflict between self-motion cues and feedback from external landmarks. In an augmented-reality system, visual landmarks were moved in proportion to the movement of a rat on a circular track, creating continuous conflict with path integration. Sustained exposure to this cue conflict resulted in predictable and prolonged recalibration of the path-integration gain, as estimated from the place cells after the landmarks were turned off. We propose that this rapid plasticity keeps the positional update in register with the movement of the rat in the external world over behavioural timescales. These results also demonstrate that visual landmarks not only provide a signal to correct cumulative error in the path-integration system[4,8,16–19], but also rapidly fine-tune the integration computation itself.

Path integration is an evolutionarily conserved strategy that enables an organism to maintain an internal representation of its current location by integrating, over time, a movement vector that represents distance and direction travelled[4–7]. Place cells and entorhinal grid cells have been implicated as key components of a path-integration system in the mammalian brain[20–22]. We recorded place cells from the hippocampal region CA1 (Extended Data Fig. 1) in five rats as they ran laps on a circular track of diameter 1.5 m. The track was enclosed within a planetarium-style dome, in which an array of three visual landmarks was projected onto the interior surface to create an augmented-reality environment (Fig. 1a, b). In contemporary virtual-reality systems[3,23–25], head- or body-fixed rats fictively locomote on a stationary air-cushioned ball or treadmill. Notwithstanding the flexibility of these systems to manipulate the visual experience of the rat, we built the dome apparatus to instead more-completely preserve natural self-motion cues, such as vestibular, proprioceptive and motor efference copy. This system enabled us to test the a priori hypothesis that manipulating the perceived movement speed of the rat relative to the landmarks results in a predictable recalibration of the path-integration gain.

To create the visual illusion that the rat was running faster or slower, the array of landmarks was rotated coherently as a function of the movement speed of the rat. Movement of the landmarks was controlled by an experimental gain, G, which set the ratio between the rat's travel distance with respect to the landmarks (landmark reference frame) and its travel distance along the stationary circular track (laboratory reference frame) (Fig. 1c). Recording sessions began with $G = 1$ (epoch 1), a control condition with landmarks held stationary, so that the rat travelled the same distance in both the landmark and the laboratory frames (Fig. 1d). The gain was then ramped over the course of several laps (epoch 2) to values less than or greater than one. For $G < 1$, the landmarks moved at a speed proportional to (but slower than) the rat in the same direction; the rat therefore ran a shorter distance in the landmark frame than in the laboratory frame. For $G > 1$, the landmarks moved in the opposite direction, meaning that the rat ran a greater distance in the landmark frame than in the laboratory frame. In epoch 3, G was held at a steady-state target value (G_{final}). In some sessions, the landmarks were then turned off (epoch 4) to assess whether the effects of gain adjustment persisted in the absence of the landmarks.

Under gain-adjusted conditions, CA1 units (7.2 ± 5.8 (mean $\pm$ s.d.) units per session) tended to fire in normal, spatially specific place fields when the firing was plotted in the landmark frame, but not when plotted in the laboratory frame (Fig. 1e). The strength and continuity of visual cue control over the place fields is highlighted by special cases of G (Fig. 2). As G was ramped down to zero, the place fields became increasingly large in the laboratory frame, eventually spanning several laps (Fig. 2a, Supplementary Video 1), but they maintained normal spatial selectivity in the landmark frame (Fig. 2b). At $G = 0$, the position of the rat became locked to the landmark frame, as the landmarks moved in precise register with the rat. Consequently, a unit that was active at that moment would typically remain active throughout epoch 3 (for example, yellow unit in Fig. 2a); by contrast, a unit that was inactive at that moment would typically remain silent throughout epoch 3 (for example, red unit in Fig. 2a). When G was clamped at integer ratios—such as 3/1 (Fig. 2c) or 1/2 (Fig. 2e)—the units maintained the typical pattern of one field per lap in the landmark frame, while firing at the expected periodicity (such as three times per lap (Fig. 2d) or every other lap (Fig. 2f)) in the laboratory frame. Remapping events sometimes caused different populations of place cells to be active at different times. For example, place cells that were active during the initial part of the session sometimes went silent (loss of field; Fig. 2e, yellow unit), and place cells that were silent during the initial part of the session sometimes began firing at a preferred location (gain of field; Fig. 2e, red unit). The remapped cells exhibited normal place fields only in the landmark frame. These examples illustrate that the landmark array exercised robust control over the place fields, outweighing any subtle, local cues on the apparatus as well as nonvisual path-integration cues, such as vestibular or proprioceptive cues.

To quantify the degree of landmark control over the population of recorded place cells, we developed a decoding algorithm that was robust to the remapping events described above. We estimated the gain, H_i, for each individual unit, i, by measuring its spatial frequency (that is, the frequency of repetition of its spatially periodic firing pattern).

[1]Department of Mechanical Engineering, Johns Hopkins University, Baltimore, MD, USA. [2]Zanvyl Krieger Mind/Brain Institute, Johns Hopkins University, Baltimore, MD, USA. [3]Department of Psychology, UCLA, Los Angeles, CA, USA. [4]Laboratory for Computational Sensing and Robotics, Johns Hopkins University, Baltimore, MD, USA. [5]Solomon H. Snyder Department of Neuroscience, Johns Hopkins University, Baltimore, MD, USA. [6]These authors contributed equally: Ravikrishnan P. Jayakumar, Manu S. Madhav. [7]These authors jointly supervised this work: Noah J. Cowan, James J. Knierim. *e-mail: manusmad@gmail.com

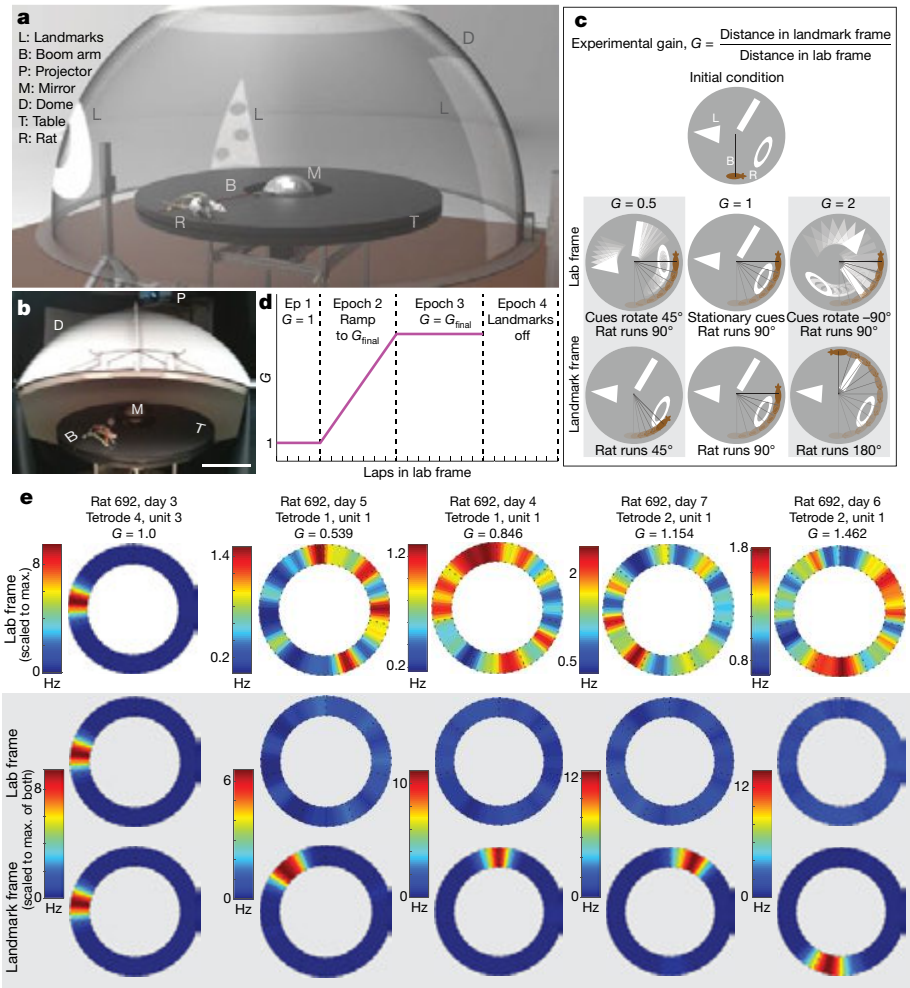

Fig. 1 | Dome apparatus, experimental procedure and sample data. **a**, Semi-transparent illustration of the dome apparatus. **b**, Photograph of the apparatus. The dome is raised to enable visualization of the interior, but it is lowered as in **a** for the experiment. Scale bar, 0.5 m. **c**, Illustration of experimental gain *G*. From the same initial positions of the landmarks and rat, three gain conditions are shown, in both laboratory (lab; top) and landmark (bottom) frames of reference. In each case, the rat runs 90° in the laboratory frame. **d**, Profile of gain change and epochs during a typical session. An annular ring is always projected at the top of the dome (as shown in **a**) for illumination purposes, and is not turned off even in epoch 4. **e**, Representative firing-rate maps for five different units from five separate gain-manipulation sessions, shown in the laboratory frame (top and middle rows) and landmark frame (bottom row) during epoch 3 (constant experimental gain). Plots in the top row are colour-scaled to their own individual maximum firing rates; plots in the middle and bottom rows are colour-scaled to the maximum firing rate of the bottom plot of each pair.

The median value of H_i over all simultaneously recorded active units during a given set of laps was taken as a population estimate of the hippocampal gain, H, for those laps. Just as G quantifies the ratio between the travel distance of the rat in the landmark frame and that in the laboratory frame, H quantifies the ratio between the travel distance of the rat in the internal hippocampal 'cognitive map' frame[1] and that in the laboratory frame. An ensemble coherence score for each unit was computed as the mean value over the session of $|1 - H_i/H|$, measuring the deviation of H_i from H (Methods). The distribution of coherence scores (Fig. 2g) shows that H_i was within 2% of H for 80% (399/500) of individual units, and deviations of more than 5% were rare. Even when individual cells remapped, they still exhibited spatial periodicity at gain factors H_i that were close to H (see red and yellow units in Fig. 2c). Therefore, the population of place cells acted as a rigidly coordinated ensemble from which a precise estimate of H could reliably be computed, despite occasional remapping by some place cells.

The degree of cue control in each session was quantified by the mean ratio H/G for epochs 1–3 of a session; a ratio close to 1 indicates that the cognitive map was anchored to the landmark frame (that is, $G \approx H$). The majority of sessions (83.33%) exhibited H/G values close to 1, but the remainder showed substantially larger ratios ($H/G > 1.1$), which indicates loss of landmark control (Fig. 2h, Extended Data Fig. 2). For sessions with $H/G < 1.1$, the spatial information per spike in the landmark frame far exceeded that in the laboratory frame (Fig. 2i). Further quantitative analysis was restricted to these sessions that demonstrated landmark control. These results indicate that the augmented reality dome was successful in producing the desired illusion by strongly controlling the spatial firing patterns of the hippocampal cells in the majority of sessions (Extended Data Figs. 3, 4).

Despite strong cue control in the majority of sessions, place fields nonetheless tended to drift systematically by a small amount against the landmark frame on each successive lap (Extended Data Fig. 5; also visible in Figs. 2a, c, e, 3a, b) leading to total drifts of up to 80° over the course of a session. The direction of this bias was consistent with a continuous conflict between the dynamic landmark reference frame and an estimate of position based on path integration (although we cannot rule out the possible contribution of subtle uncontrolled external cues on the track or in the laboratory). That is, when path integration presumably undershot the landmark-defined location systematically ($G < 1$), the place fields shifted slightly backwards in the landmark frame; conversely, when path integration overshot the landmarks ($G > 1$), the place fields shifted forward. The shift may reflect a conflict resolution that is weighted heavily, but not completely, in the direction predicted by the landmark frame.

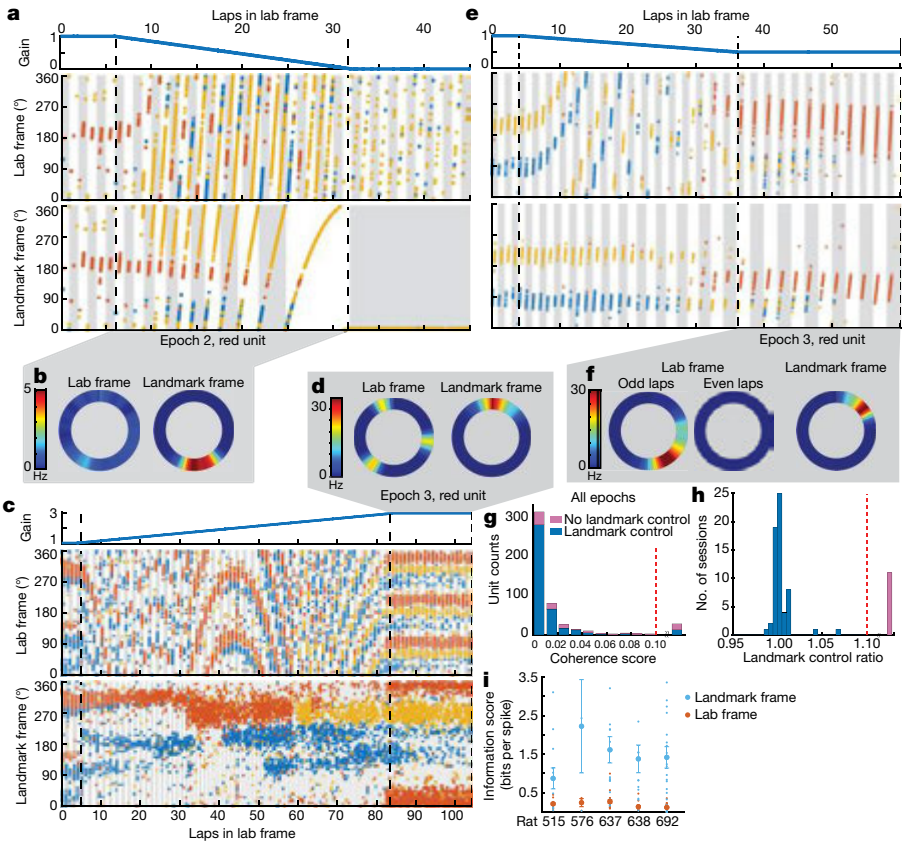

Fig. 2 | Control of place fields by landmarks. a, Top, profile of experimental gain, *G*, for epochs 1–3 of a session in which G_{final} was 0. Middle, coloured dots show the location of the rat in the laboratory frame (*y* axis) as a function of cumulative distance travelled on the track (*x* axis) when spikes from three units (red, blue and yellow) were recorded. Alternate grey and white bars indicate laps in this frame. Bottom, the same spikes in the landmark frame. Alternate grey and white bars indicate laps in this frame. The yellow unit fired weakly during the first 8 laps, became stronger on laps 9–10, and maintained the strong field in the landmark frame throughout the remainder of the session. During the last landmark-frame lap, the unit fired in a field that spanned roughly 1,080° (3 laps) in the laboratory frame (middle). **b**, Rate maps of the red unit in laboratory and landmark frames for epoch 2 of the session shown in **a**. The firing rate is low and diffusely distributed (on average) in the laboratory frame, whereas there is a well-defined place field in the landmark frame. **c**, Epochs 1–3 of a session in which G_{final} was 3 (same format as **a**). In epoch 3, all 3 units maintain normal spatial firing in the landmark reference frame, but they have 3 fields per lap (separated by 120°) in the laboratory frame. **d**, Rate maps of the red unit for epoch 3 of the session shown in **c**. **e**, Epochs 1–3 of a session in which G_{final} was 0.5. Remapping occurred near the transition between epoch 2 and epoch 3, as the previously silent red unit became active and maintained a stable place field in the landmark frame. In the laboratory frame, however, the unit fired every other lap (that is, it was active on the grey laps and silent on the intervening white laps). **f**, Rate maps for the red unit for epoch 3 of the session shown in **e**. Separate rate maps are shown for the odd- and even-numbered laps in the laboratory frame. **g**, Coherence of the population response. The $n = 500$ units acted as a coherent population in sessions with (blue, 411/500) and without (pink, 89/500) landmark control (see **h**). Units with a coherence score of greater than 0.1 (range 0.12–0.47) were combined in a single bin (29/500 units). These cells generally displayed poor spatial tuning and therefore did not admit a reliable estimate of hippocampal gain. **h**, Landmark control ratio. In most sessions (blue, 60/72 sessions), the landmark control ratio was approximately 1. Sessions with a gain ratio of greater than 1.1 (range 1.16–4.02) were combined in a single bin (pink, 12/72 sessions). **i**, Spatial information scores in the laboratory and landmark frames for each rat (sessions with $n = 12, 3, 17, 15, 29$ units) are significantly different (two-sided paired *t*-test, $n = 5$ rats, $t_4 = 6.213$, $P = 0.0034$). Data are mean ± s.e.m, with scores from individual units shown.

Given the apparent influence of path integration on place cells, as revealed by systematic place-field drift despite strong landmark control, we tested whether the sustained exposure to the cue conflict induced a recalibration of the path integrator that persisted in the absence of landmarks. Such recalibration would be evidenced by a predictable change in the hippocampal gain when visual landmarks were turned off (Fig. 1d, epoch 4). The baseline hippocampal gain *H* was measured for each rat after the removal of landmarks in sessions in which the rat ran approximately 30 laps with stationary landmarks ($G = 1$). As expected, the baseline value of *H* was close to 1 (range 0.997–1.036). In subsequent gain-manipulation sessions, if the path-integrator circuit were unaltered it would be expected that the place fields would revert to the laboratory frame ($H \approx 1$) when the landmarks were turned off, as in the baseline sessions. Alternatively, if the path-integrator gain were recalibrated perfectly, one would expect that the place fields would continue to fire as if the landmarks were still present and rotating at the final experimental gain (that is, $H \approx G_{final}$). We found that the hippocampal representation during epoch 4 was intermediate between these extremes (Fig. 3a, b, Supplementary Video 2): there was a clear, linear relationship between G_{final} and the *H* estimated during the first 12 laps after the landmarks were turned off (Fig. 3c). Moreover, this linear relationship was maintained when *H* was estimated during the next 12 laps (Extended Data Fig. 6f). The values of *H* for the first and second 12 laps were highly correlated (Fig. 3d) with a slope near to 1 (1.03). Therefore, *H* was stable over at least 18 laps (that is, the middle of the second 12-lap estimation window). Despite this overall stability, there were still fluctuations in *H* in the absence of landmarks (Fig. 3e, Extended Data Fig. 6). We tested whether changes in behaviour could account for the hippocampal-gain recalibration by computing several behavioural measures for each epoch (Extended Data Table 1, see 'Behavioural analysis' in Methods). Multiple regression analysis showed that G_{final} strongly predicted *H*, whereas the behavioural variables had negligible influences on *H* (Extended Data Table 1).

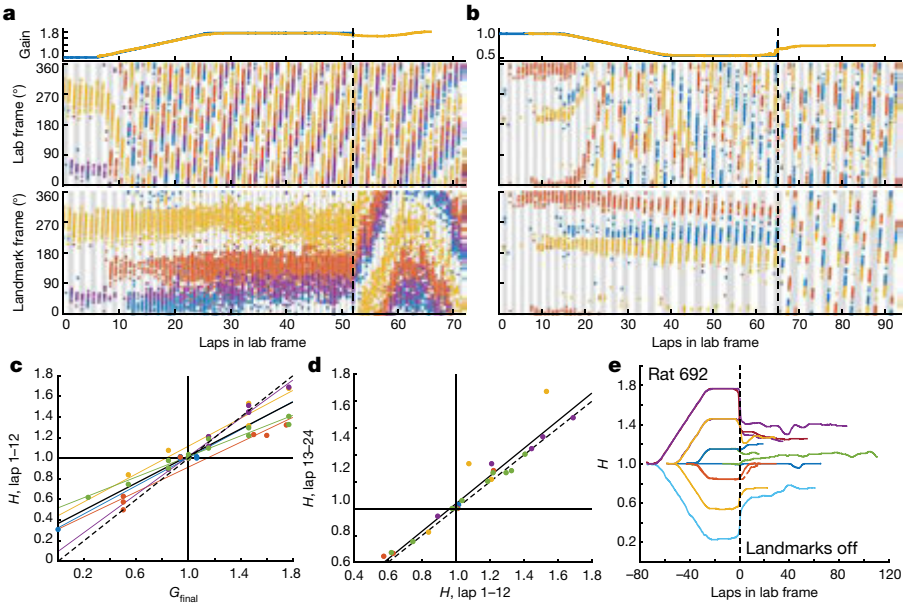

Fig. 3 | Recalibration of place fields by landmarks. a, Example of positive recalibration. Top, experimental gain, *G* (blue) and hippocampal gain, *H* (yellow) for epochs 1–3 of a session in which G_{final} was 1.769. Middle, spikes from three putative pyramidal cells (blue, red and yellow dots) in the laboratory frame. Bottom, the same spikes in the landmark frame. When the landmarks were turned off (dashed line, epoch 4), *H* remained close to G_{final}, shown by the slower drift of the place fields in the landmark frame compared to the laboratory frame. During epoch 4, the landmark frame was defined assuming the gain was G_{final}, even though landmarks were off. Note that the traces of *H* deviate from those of *G* before the landmarks are turned off; this is an artefact of the sliding window used in the spectrogram and does not affect the conclusions (see Methods, 'Visualizing *H*'). **b**, Example of negative recalibration. G_{final} was 0.539. **c**, Recalibration of place fields. Values of *H* were computed using the first 12 laps (that is, the value of *H* at lap 6) after the landmarks were turned off. Linear fits for each rat (colour) and for the whole dataset (black) are shown ($n = 45$ sessions, Pearson's $r_{43} = 0.94$, $P = 3.4 \times 10^{-21}$), along with the perfect recalibration line (dashed line, black). Note that the linear fit passes close to the origin, showing that $H \approx 1$ when the landmarks were turned off after baseline control experiments. **d**, The stability of recalibration, shown by a comparison of *H* during laps 1–12 and *H* during laps 13–24. The linear fit is shown in black ($n = 27$ sessions, Pearson's $r_{25} = 0.96$, $P = 1.16 \times 10^{-15}$). **e**, Complete gain dynamics for one rat. For all recalibration sessions from one rat, *H* is plotted as a function of laps run in the laboratory frame. All the sessions are aligned to the instant when the landmarks were turned off (lap 0). The recalibrated *H* was maintained for up to 50 laps or more.

Using an augmented-reality dome apparatus, we show here that the path-integration system uses a modifiable gain factor that can be recalibrated to a new value that can remain stable for at least several minutes in the absence of salient landmarks. Recalibration of this nature has been described extensively in other systems. The cerebellum has a key role in recalibration of feedforward motor commands[26]. Similarly, the gain of the vestibulo-ocular reflex adapts to changes in the magnitude of retinal slip caused by magnifying glasses, an effect that persists even after the glasses are removed[27]. As with our own results, the recalibration is not perfect in these motor adaptation tasks; that is, the gain measured after the training sessions are biased towards, but not precisely the same as, the experimental gain implemented during the training sessions. To our knowledge, such gain recalibration has not been demonstrated physiologically in cognitive phenomena such as spatial representation and path integration (although see ref. [15]). The lack of complete recalibration observed in our experiment may be due to an insufficient number of training laps during epoch 3, or may reflect inherent limits on the plasticity of the path-integrator gain variable.

It is widely accepted that visual landmarks provide a signal to correct the error that accumulates during path integration[19]. The results in this paper demonstrate physiological evidence for a role of vision in the path-integration computation itself by providing an error signal that is analogous to retinal slip in the vestibulo-ocular reflex[27]. Specifically, this error signal fine-tunes the gain of the path integrator[15], which minimizes the accumulation of error in the first place. Although recalibration of the path-integrator gain may be expected over developmental timescales, these results indicate that the path-integration gain is fine-tuned even at behavioural timescales. This fine-tuning may be required for several reasons: to maintain the accuracy of the path-integration signal under different behavioural conditions (for example, locomotion on different surfaces that provide varying degrees of slip and cause alterations in the self-motion inputs to the path integrator); to synchronize the different types of self-motion signals (for example, vestibular, optic flow, motor copy or proprioception) that are thought to underlie path integration; and to coordinate the discrete set of different path-integration gains that are thought to underlie the expansion of grid scales along the dorsal–ventral axis of the medial entorhinal cortex[12,28,29]. The recalibration might be implemented by changes to the head-direction[30] or speed[31,32] signals that provide input to a path-integration circuit. Alternatively, these representations may be unaltered and the gain changes implemented by changing the synaptic weights between the inputs and putative attractor networks that perform the path integration[9–11,13]. The augmented-reality system described here will enable the investigation of mechanisms that underlie the interaction between external sensory input and the internal neural dynamics at the core of the path-integration system.

Online content

Any methods, additional references, Nature Research reporting summaries, source data, statements of data availability and associated accession codes are available at https://doi.org/10.1038/s41586-019-0939-3.

Received: 15 April 2018; Accepted: 10 January 2019;
Published online 11 February 2019.

1. O'Keefe, J. & Nadel, L. *The Hippocampus as a Cognitive Map* (Oxford Univ. Press, Oxford, 1978).
2. Acharya, L. et al. Causal influence of visual cues on hippocampal article causal influence of visual cues on hippocampal directional selectivity. *Cell* **164**, 197–207 (2016).
3. Chen, G., King, J. A., Burgess, N. & O'Keefe, J. How vision and movement combine in the hippocampal place code. *Proc. Natl Acad. Sci. USA* **110**, 378–383 (2013).
4. Etienne, A. S. & Jeffery, K. J. Path integration in mammals. *Hippocampus* **14**, 180–192 (2004).

5. Wehner, R. & Menzel, R. Do insects have cognitive maps? *Annu. Rev. Neurosci.* **13**, 403–414 (1990).
6. Wittlinger, M., Wehner, R. & Wolf, H. The ant odometer: stepping on stilts and stumps. *Science* **312**, 1965–1967 (2006).
7. Mittelstaedt, M. L. & Mittelstaedt, H. Homing by path integration in a mammal. *Naturwissenschaften* **67**, 566–567 (1980).
8. Gallistel, C. R. *Learning, development, and conceptual change. The organization of learning* (MIT Press, Cambridge, 1990).
9. Samsonovich, A. & McNaughton, B. Path integration and cognitive mapping in a continuous attractor neural network model. *J. Neurosci.* **17**, 5900–5920 (1997).
10. Fuhs, M. C. & Touretzky, D. S. A spin glass model of path integration in rat medial entorhinal cortex. *J. Neurosci.* **26**, 4266–4276 (2006).
11. McNaughton, B. L., Battaglia, F. P., Jensen, O., Moser, E. I. & Moser, M. B. Path integration and the neural basis of the 'cognitive map'. *Nat. Rev. Neurosci.* **7**, 663–678 (2006).
12. Hasselmo, M. E., Giocomo, L. M. & Zilli, E. A. Grid cell firing may arise from interference of theta frequency membrane potential oscillations in single neurons. *Hippocampus* **17**, 1252–1271 (2007).
13. Blair, H. T., Gupta, K. & Zhang, K. Conversion of a phase- to a rate-coded position signal by a three-stage model of theta cells, grid cells, and place cells. *Hippocampus* **18**, 1239–1255 (2008).
14. Burgess, N., Barry, C. & O'Keefe, J. An oscillatory interference model of grid cell firing. *Hippocampus* **17**, 801–812 (2007).
15. Tcheang, L., Bulthoff, H. H. & Burgess, N. Visual influence on path integration in darkness indicates a multimodal representation of large-scale space. *Proc. Natl Acad. Sci. USA* **108**, 1152–1157 (2011).
16. Knierim, J. J., Kudrimoti, H. S. & McNaughton, B. L. Interactions between idiothetic cues and external landmarks in the control of place cells and head direction cells. *J. Neurophysiol.* **80**, 425–446 (1998).
17. Zugaro, M. B., Arleo, A., Berthoz, A. & Wiener, S. I. Rapid spatial reorientation and head direction cells. *J. Neurosci.* **23**, 3478–3482 (2003).
18. Hardcastle, K., Ganguli, S. & Giocomo, L. M. Environmental boundaries as an error correction mechanism for grid cells. *Neuron* **86**, 827–839 (2015).
19. Etienne, A. S., Maurer, R. & Séguinot, V. Path integration in mammals and its interaction with visual landmarks. *J. Exp. Biol.* **199**, 201–209 (1996).
20. Moser, E. I., Moser, M.-B. & McNaughton, B. L. Spatial representation in the hippocampal formation: a history. *Nat. Neurosci.* **20**, 1448–1464 (2017).
21. Gil, M. et al. Impaired path integration in mice with disrupted grid cell firing. *Nat. Neurosci.* **21**, 81–93 (2018).
22. Tennant, S. A. et al. Stellate cells in the medial entorhinal cortex are required for spatial learning. *Cell Rep.* **22**, 1313–1324 (2018).
23. Hölscher, C., Schnee, A., Dahmen, H., Setia, L. & Mallot, H. A. Rats are able to navigate in virtual environments. *J. Exp. Biol.* **208**, 561–569 (2005).
24. Harvey, C. D., Collman, F., Dombeck, D. A. & Tank, D. W. Intracellular dynamics of hippocampal place cells during virtual navigation. *Nature* **461**, 941–946 (2009).
25. Ravassard, P. et al. Multisensory control of hippocampal spatiotemporal selectivity. *Science* **340**, 1342–1346 (2013).
26. Bastian, A. J. Learning to predict the future: the cerebellum adapts feedforward movement control. *Curr. Opin. Neurobiol.* **16**, 645–649 (2006).
27. Miles, F. A. & Lisberger, S. G. Plasticity in the vestibulo-ocular reflex: a new hypothesis. *Annu. Rev. Neurosci.* **4**, 273–299 (1981).
28. Terrazas, A. et al. Self-motion and the hippocampal spatial metric. *J. Neurosci.* **25**, 8085–8096 (2005).
29. Maurer, A. P., VanRhoads, S. R., Sutherland, G. R., Lipa, P. & McNaughton, B. L. Self-motion and the origin of differential spatial scaling along the septo-temporal axis of the hippocampus. *Hippocampus* **15**, 841–852 (2005).
30. Cullen, K. E. & Taube, J. S. Our sense of direction: progress, controversies and challenges. *Nat. Neurosci.* **20**, 1465–1473 (2017).
31. Kropff, E., Carmichael, J. E., Moser, M.-B. & Moser, E. I. Speed cells in the medial entorhinal cortex. *Nature* **523**, 419–424 (2015).
32. Hinman, J. R., Brandon, M. P., Climer, J. R., Chapman, G. W. & Hasselmo, M. E. Multiple running speed signals in medial entorhinal cortex. *Neuron* **91**, 666–679 (2016).

Acknowledgements We thank B. Nash and B. Quinlan for assistance with constructing the apparatus; M. Ferreyros, M. Breault, N. Lukish, J. Johnson, B. Vagvolgyi and D. GoodSmith for technical assistance in running experiments; and G. Rao, V. Puliyadi, C. Wang, H. Lee, R. Nickl, A. Haith and J. Bohren for discussions and technical advice. This research was supported by National Institutes of Health grants R01 MH079511 (H.T.B., J.J.K.), R21 NS095075 (N.J.C., J.J.K.), and R01 NS102537 (N.J.C., J.J.K., F.S.), a Johns Hopkins University (JHU) Discovery Award (N.J.C., J.J.K.), a JHU Science of Learning Institute Award (J.J.K., N.J.C.), a JHU Kavli NDI Postdoctoral Distinguished Fellowship (M.S.M.) and a JHU Mechanical Engineering Departmental Fellowship (R.P.J.).

Author contributions J.J.K., N.J.C. and H.T.B. conceived and all authors designed the study. J.J.K. and N.J.C. advised on all aspects of the experiments and analysis. F.S. made key contributions to the analysis and interpretation of the data and provided supervision over data acquisition and analysis. R.P.J. and M.S.M. designed and constructed the apparatus, performed experiments and analysed the data. R.P.J., M.S.M., N.J.C. and J.J.K. wrote the paper, and F.S. and H.T.B. provided critical feedback.

Competing interests The authors declare no competing interests.

Additional information
Extended data is available for this paper at https://doi.org/10.1038/s41586-019-0939-3.
Supplementary information is available for this paper at https://doi.org/10.1038/s41586-019-0939-3.
Reprints and permissions information is available at http://www.nature.com/reprints.
Correspondence and requests for materials should be addressed to M.S.M.
Publisher's note: Springer Nature remains neutral with regard to jurisdictional claims in published maps and institutional affiliations.

METHODS

Subjects. Five male Long–Evans rats (Envigo Harlan) were housed individually on a 12:12 h light:dark cycle. All training and experiments were conducted during the dark portion of the cycle. The rats were 5–8 months old and weighed 300–450 g at the time of surgery. All animal care and housing procedures complied with National Institutes of Health guidelines and followed protocols approved by the Institutional Animal Care and Use Committee at Johns Hopkins University.

Dome apparatus. The augmented-reality dome apparatus that we designed for this experiment is similar to a planetarium. The hemispherical dome (2.3-m inner diameter) was constructed from fibreglass (Immersive Display). The inside surface was uniformly coated with a 50% reflective paint (RAL7040 grey). A hole (15-cm diameter) at the top of the dome enabled light from a video projector (Sony VPL-FH30) with a long-throw lens (Navitar ZM 70-125 mm) to enter. Visual cues were projected onto the inside surface of the dome (Fig. 1). An annular ring of light was projected onto the top, interior surface of the dome; when the spatial landmarks were turned off in epoch 4, this ring remained on to provide non-directional illumination.

An annular table (152.4-cm outer diameter, 45.7-cm inner diameter) was centred within the dome. The support legs of the dome and the legs of the table were not visible to the rat during the experiment. A commutator (PSR-36, Neuralynx) was mounted in the centre of, but slightly below, the tabletop. The commutator drum was upward, inverted from the typical, ceiling-mounted installation. A hemispherical first-surface mirror (25-cm diameter; JR Cumberland) was mounted to the commutator drum. The image from the projector was reflected off of the mirror and onto the interior surface of the dome. A radial arm (6-mm carbon-fibre rod) extending almost to the edge of the table was attached to the central commutator through a smooth bearing. The angle of rotation between the arm and the commutator drum was monitored by a built-in optical encoder. A microcontroller actuated a stepper motor attached to the commutator drum to maintain this angle close to zero, effectively rotating the drum of the commutator along with the radial arm. The rate of rotation of the motor, and correspondingly its auditory noise frequency, was proportional (up to a saturation point) to the speed of the rat in the laboratory frame. The noise could thus potentially serve as an artificial (learned) self-motion cue. If so, the results indicate either that this cue is inconsequential for updating path integration or it is recalibrated along with the natural self-motion cues (that is, vestibular, motor copy, proprioception and so on.).

Two 3D-printed 'chariot' arms for harnessing the rat were attached to the radial arm near the edge of the table. Other lightweight 3D-printed components were sometimes attached to the radial boom arm to affix infrared lights, feeding tubes, recording tether supports and so on. The rat wore a body harness (Coulbourn Instruments), onto which Velcro strips and a magnetic attachment pad were sewn. The magnets helped to align the harness to paired magnets attached to the chariot arms and the Velcro strip held the rat in that position relative to the arms. During the experiment, the rat pulled the arm and the components attached to it. Owing to the long lever provided by the radial arm and the smooth bearing attachment to the commutator, the load borne by the rat was minimal.

A liquid-reward vial, pump and a battery to power the pump and infrared lights were mounted to the commutator drum. The commutator drum was connected to a second optical encoder (Hohner, series INSQ) that measured its angular displacement relative to the table. Hence, the angle of the rat in the laboratory frame was the sum of the angle measurement from the two encoders (that is, the angle of the commutator relative to the table and the angle of the radial arm relative to the commutator). A Hall-effect sensor (55100-3H-02-D, Littelfuse) mounted to the table, and a corresponding magnet mounted to the commutator drum, were used for post hoc detection and correction of any spurious jumps in the angle of the rat. To mask auditory cues emanating from outside the dome during the experiments, white noise was played by a speaker placed centrally underneath the table.

A camera was mounted next to the hole at the top of the dome and was hidden from the rat using an annular, concentrically mounted one-way mirror that encircled the hole, occluding the camera from view. The camera provided an overhead view of each experiment, which enabled observation of the experiments and intervention by the experimenter when necessary (for example, if the rat broke free from the harness). During the experiments, synchronized video of the rat's behaviour was recorded. To verify our ability to track the angle of the rat, we tracked the location of the boom arm post hoc using the video recording. We implemented a template-based tracking algorithm using standard subroutines in the freely available OpenCV library (opencv.org, v.3.2.0). On the basis of the camera resolution (1,024 × 768 for the first two rats and 2,048 × 2,048 for the last three rats), each pixel was calculated to correspond to $<1°$ of the track. The mean absolute error between the video-based tracking and the encoder-based rat angle was small (mean: 3.60° ± 3.86° s.d.) across all 72 sessions.

Training. Over 2–3 days, we familiarized the rats to human contact and to wear the body harness. The rats were placed on a controlled feeding schedule to reduce their weights to approximately 80% of their ad libitum weight, whereupon they were trained to run for a food reward (either Yoo-hoo or 50% diluted Ensure) on a training table in a different room from the experimental room. Reward droplets were manually placed at arbitrary locations on the track in the path of the running rat, and the experimenter attempted to lengthen the average interval between rewards to maintain behaviour while prolonging satiation. The rats were then transitioned to automatic feeding, in which a liquid reward was dropped at intervals that varied over time as the behaviour of the rats was shaped to maximize forward movement with minimal pauses. The training setup had a similar radial arm and chariot to the main apparatus, but without the surrounding virtual environment. Once the rats were consistently running 30–40 laps without human intervention on the training table, we moved them into the dome and trained them until they ran 30–40 laps in the presence of stationary visual cues. Training usually took 2–3 weeks.

Electrode implantation and adjustment. After training, rats were implanted with hyperdrives containing 6 (2 rats) or 12 (3 rats) independently movable tetrodes. Following surgery, 30 mg of tetracycline and 0.15 ml of a 22.7% solution of the antibiotic enrofloxacin were administered orally to the rats each day. After at least four days of recovery, we began slowly advancing the tetrodes and resumed food restriction and training within seven days of surgery. Once the tetrodes were close to CA1 they were advanced less than 40 μm per day. Once the tetrodes were judged to be in CA1, as confirmed by sharp waves and ripples in electroencephalogram (EEG) signals and the presence of isolatable units, and the rat was again running at least 30 laps inside the dome, the experimental sessions began.

Neural recording. During sessions, the rat was attached to the chariot arms and a unity-gain headstage was attached to its implanted hyperdrive. The neural signals passed through the commutator and were filtered (600–6,000 Hz), digitized at 30 kHz, and recorded on a computer running the Cheetah 5 recording software (Neuralynx). Simultaneously, EEG data from each tetrode was filtered (1–475 Hz), digitized at 30 kHz, and stored on the computer. Pulses sent from the experiment-control computer (see section 'Experimental control') were time-stamped and recorded as events on the neural-recording computer to enable the post hoc synchronization of the data streams recorded on the two computers.

Experimental control. A data acquisition system (National Instruments, NI PCIe-6259) was used to communicate with the dome apparatus. The experiment was controlled by a custom software system coordinated by the software development framework called Robot Operating System[33] (ROS, Open Source Robotics Foundation, distributed under the BSD-3-Clause License) on a computer running the Linux Operating System (Ubuntu 12.04, 14.04). The custom ROS-based system received information about the angular position of the rat from the two optical encoders and generated the visual scene using standard open-source OpenGL C++ libraries. The visual scene was deformed to match the optics of the projection system and displayed on the projector mounted above the dome. The experimentally measured time lag between movement of the boom arm and movement of the landmark array was 97 ± 24 ms (s.d.). The time lag was due to processing time delays as well as to the frame rate of the video projector (17 ms per frame); the jitter was due to occasional frame drops and inconsistencies in update rate due to momentary computational demands (data not shown). We also computed where the landmarks should have been projected if we had instantaneous control. There was no detectable slippage (drift) between the intended location of landmarks and where they were actually projected. The mean absolute error between these values was small for all sessions in which the landmarks were moving (that is, non-control sessions) (54/72 sessions; mean: 0.59 ± 0.43° (s.d.); max: 1.69°).

Rats were rewarded by automatically dropping liquid reward at pseudo-random spatial intervals in the laboratory frame. These intervals were picked from a uniform distribution with means (typically 40–80°) specified at the beginning of each session. The mean feeding interval was increased gradually during training to delay satiation and maintain running performance, and was generally constant during each experimental session. The experimenter could also dispense reward manually to encourage running behaviour when necessary. All the data, including position of the rat, position of the visual stimuli, reward locations and the overhead video, were saved during the course of the session.

Experimental procedure. On each experimental day, baseline data were recorded from the rat for 20 min before and after the session while it slept or rested quietly in a towel-lined dish on a pedestal. These sleep data were used post hoc to confirm the recording stability of single units during the sessions. During the sessions, the experimenter went into the dome with the rat and always attached the rat to the harness at the same starting location relative to the landmarks (which were always located at the same locations relative to the laboratory frame). After ensuring that the rat was running with a natural gait, the experimenter left the dome. The progress of the session was monitored using the overhead camera, and the experimenter only interfered in cases when the rat partially broke free of the harness, stopped running for long periods or was running with an unnatural gait.

The session duration varied depending on the running speed of the rat and on how many laps were planned for that session (for example, ramps to smaller gain values required fewer laps in total to complete the experiment). On days with

short sessions, a second session was sometimes held after a short rest duration. The rat was taken out and placed on the pedestal between sessions, to keep the initial conditions consistent. Except on some days in which landmarks were kept stationary for the whole duration of the session, we took the rat out of the dome only during epoch 4 (no landmarks inside dome).

Experimental gain selection and gain ramp rates. Each rat initially ran 1–3 sessions in which the landmarks were stationary. In most of these sessions, rats first ran 30 laps with stable landmarks ($G = 1$) to mimic the number of laps in epoch 3 for our regular recalibration sessions, and then they ran 30 laps with the landmarks turned off. After these initial days, on subsequent days of recording the value of G was varied away from 1. For the first rat (515), we chose values of G close to 1 (1.0625, 0.9375), in addition to one session with a gain of 0. For the second rat (576) we typically used gains 0.25, 0.5 and 0.75, which resulted in periodic repetitions of place fields in the laboratory frame. For the remaining three rats, to reduce ambiguity between firing patterns in the laboratory and landmark frames of reference, gains were selected in the form of $1 \pm n/13$, $n = 2, 6, 10$, resulting in gains of 0.231, 0.539, 0.846, 1.154, 1.462 and 1.769. These values ensured that during epoch 3 the position of the rat relative to the laboratory and landmark frames of reference aligned only once every 13 laps. We used gain ramp rates during epoch 2 ranging from 1/128 to 1/26 (gain change per lap). The number of laps in epoch 1 was different for each rat (4 laps for 515 and 576, 6 laps for 637 and 638, and 15 laps for 692). However, the number of laps in epoch 1 had no apparent relationship to the degree of cue control when the landmarks started to move (proportion of sessions with landmark control failure: 515: 0/15; 576: 1/9; 637: 4/17; 638: 3/14; 692: 3/17). The sessions were not randomized; the gain for each session was selected by hand such that gains were rarely repeated in consecutive sessions, and the gain manipulation typically increased in magnitude over consecutive sessions for any given animal. The investigators were not blinded to allocation during experiments and outcome assessment. No statistical methods were used to predetermine sample size.

Data analysis. Data from the two experiment computers were synchronized using the paired pulses, and all data were transformed into the same set of timestamps. For each triggered spike waveform, features such as peak, valley and energy were used to sort spikes using a custom software program (WinClust; J.J.K.). Cluster boundaries were drawn manually on two-dimensional projections of these features from two different electrodes of a tetrode. We mostly used maximum peak and energy as features of choice; however, other features were used when they were required to isolate clusters from one another. Clusters were assigned isolation quality scores ranging from 1 (very well isolated) to 5 (poorly isolated) agnostic to their spatial-firing properties. Only clusters rated 1–3 were used for all quantitative analyses in the main text.

To be included in the quantitative analyses, sessions were required to meet the following criteria: sessions with landmark manipulation were completed and the rat was removed in the absence of landmarks; and there were no major behavioural issues or long manual interventions during the session. For the 72/88 sessions that met these criteria, spikes that occurred when the movement speed of the rat was less than 5° s^{-1} (about 5 cm s^{-1}) were removed. For each unit, the number of spikes fired when the rat occupied a 5° bin was divided by the time the rat spent in the bin to compute the firing rate. The firing rate was further smoothed with a Gaussian filter of standard deviation 4°. Single units were classified into putative pyramidal cells and putative interneurons by separating them on the basis of firing rate, spike duration and the autocorrelation function[34]. Only the putative pyramidal cells were used for the main analyses, and the putative interneurons are described in Extended Data Fig. 7.

Spatial information scores were computed by binning and determining firing rates of spikes in both the laboratory and the landmark frames of reference, as described above. If the occupancy-corrected firing rate in bin i is λ_i, then information score is computed as:

$$\frac{1}{N}\sum_{i=0}^{N}\lambda_i \log_2 \frac{\lambda_i}{\lambda}$$

in which N is the total number of bins, and λ is the mean firing rate[35].

Behavioural analysis. For each of the four epochs, the mean running speed (cm s^{-1}), the rate of pauses in running (defined as continuous epochs of 3 s or more where the velocity decreases below 5 cm s^{-1}) (number per lap), the mean duration of each pause (s), the mean interpause temporal interval (s) and the mean interpause spatial interval (cm) were calculated. Interpause intervals were spatial or temporal differences between pause events, in which the beginning and end of an epoch were also considered pauses. We first tested whether there were statistically significant changes in these variables between epochs 1 and 3 (that is, before and after the gain ramp) and between epochs 3 and 4 (that is, before and after the landmarks were turned off). Next, to address whether changes in behaviour predicted the hippocampal gain change in epoch 4, we ran 2 multiple regression analyses. First, we subtracted the values of each of the behavioural variables in epoch 1 from the values in epoch 3. A multiple regression was run with the hippocampal gain (H) in epoch 4 as the dependent variable and the five epoch 3–epoch 1 behavioural measures, as well as the experimental gain (G) of epoch 3, as the regressors. Second, we ran a multiple regression (similar to that above) with epoch 4–epoch 3 behavioural measures, as well as the experimental gain (G) of epoch 3, as the regressors.

Estimation of hippocampal gain, *H*. The position of a rat can be decoded from a population of simultaneously recorded place cells using established techniques[36–38]. However, these techniques use an independent dataset to train an estimator and require that the spatial coding be unchanged during the testing phase. In our experiments, there were often remapping events during the gain-manipulation epochs, as some units lost their firing fields and other units—which were previously silent—gained place fields on the track. This remapping was typically not all-or-none; rather, different place fields would appear or disappear at different times in the experiments (for example, Figs. 2c, e, 3a, b). Although the new place fields changed their firing locations coherently with the existing place fields during the experimental manipulations, extensive remapping causes classic population-decoding methods to become less accurate or to fail entirely. To solve this problem, we took advantage of the periodicity of firing of the place fields as the rats ran laps on the circular track to measure the spatial frequency of the population representation. This spatial frequency is insensitive to the specific place cells that are active at any given moment and it thus forms the core of a spectral-decoding technique that is robust to remapping (Extended Data Fig. 8).

The frequency estimate is termed the hippocampal gain, H. A typical place cell with a single field on a circular track exhibits one field per lap, and hence H should be 1 (Fig. 1e). Because the visual landmarks are moved at an experimental gain G, the rat encounters each landmark every $1/G$ laps. If the place fields are controlled by landmarks—that is, they fire every lap at the same location in the landmark reference frame—the value that we estimate for H should be similar to the value of G. For example, when $G = 1/2$, there should be 1 field every 2 laps, and thus $H = 1/2$ (Fig. 2c, d), and for $G = 3$, there should be 3 firing fields per lap, and thus $H = 3$ (Fig. 2e, f).

Hippocampal gain is first estimated independently for all well-isolated units (H_i for the ith unit) that fire at least 50 spikes per session while the rat is running faster than 5° s^{-1}. The spatial spectrogram of the firing rate of each unit was computed at spatial frequencies (that is, the frequency of repetition of its spatial firing pattern per physical lap) of between 0.16 per lap and 6 per lap, using a sliding window of size 12 laps applied at increments of 5°. The spectrogram was further sharpened using the method of reassignment, which can be used when the input signal contains sparse periodic signal sources[39]. The original spectrogram was also thresholded to the mean + K times the standard deviation (K between 1.1 and 2 based on visual inspection of the raw spectrogram) of its power at each spatial window; this thresholding was then applied to the sharpened spectrogram to improve the signal-to-noise ratio of the spatial frequency content.

The spectrogram can have substantial power in the harmonics of the fundamental frequency, requiring a method to reliably find the fundamental. The gain-estimation algorithm identified peaks in the autocorrelation of the spectrogram at each spatial window. Because these peaks typically lie at the fundamental frequency and its harmonics, the fundamental frequency should be both the lowest peak and the difference between peaks. If the median of the difference between peaks was an integer multiple of the lowest peak, the lowest peak was considered the fundamental frequency, and all the power in the reassigned spectrogram further than 0.1 Hz from the fundamental was set to zero (if not, the spectrogram was used as-is). This process was repeated for each spatial window. Finally, the maximum-energy trajectory from the reassigned spectrogram was extracted, and this trajectory formed the time-varying gain estimate for that particular unit. In some cases a particular unit did not produce sufficient spiking activity to generate an estimate for a given window; entries for which there was no estimate were set to NaN in MATLAB for computational convenience. The hippocampal gain estimate for each window for the population (H) was calculated as the median H_i from all units under consideration. If there were no active units during a given window (all NaNs), then the value for H was set to NaN for that window.

Visualizing *H*. For each experimental session, H can be plotted as a function of angular displacement of the rat (for example, Fig. 3a, b, Extended Data Fig. 5a, b). It is important to note that each estimate is correlated with neighbouring estimates owing to the 12-lap sliding window. Estimates that are 12 laps apart are calculated from independent data. The estimate at any given angular position is 'non-causal' in the sense that it uses neural data from ±6 laps centred around that angular position. This creates the illusion that H 'anticipates' the removal of landmarks (Fig. 3a, b, f, Extended Data Figs. 6a–e, 7a, b). Inspection of the raw spikes readily verifies that this is an artefact, but this artefact does not affect any of the interpretations in this paper.

Coherence score. In a session, if a unit, i, is part of a coherent population, its gain should equal the hippocampal gain, namely $H_i \approx H$. Thus for each 12-lap window we computed a coherence error $|1 - H_i/H|$ and defined the coherence score as the mean of this quantity over an entire session.

Landmark control ratio. In a session, if the hippocampal gain follows the experimental gain, we expect $H/G = 1$. Thus, H/G was computed at each overlapping 12-lap window for epochs 1–3 and the landmark control ratio was defined as the average of this quantity over a session.

Analysis of drift. From each session with landmark control, we identified units that had a single, non-remapped firing field in the landmark frame during epochs 1–3. The average landmark-relative firing rate maps of each unit were calculated separately for the duration of epoch 1 (start of session, $G = 1$) and for the last 12 laps before the landmarks were turned off. The cross-correlation between these two firing rate maps was computed as the rate maps were rotated relative to each other. The landmark-relative angle lag corresponding to maximum correlation was considered to be the drift of the unit. For sessions with multiple units with firing fields that did not remap during epochs 1–3, we took the mean drift over all units to be the drift for that session. In all, this analysis used 136 units from 55 days.

Analysis of recalibration. We chose sessions with landmark control and at least 12 laps run after the landmarks were turned off (epoch 4). The recalibrated gain was selected as the value of H six laps after the landmarks were turned off (lap 6 was the midpoint of the first 12-lap window that includes only data from epoch 4). To examine the decay rate of recalibration, we chose sessions with landmark control and at least 24 laps run in epoch 4. We compared the recalibrated gain at lap 6 with the value of H at lap 18 (the first point at which the two 12-lap spectrogram windows do not overlap).

Histology. Once experimental sessions were complete, rats were transcardially perfused with 3.7% formalin. The brain was extracted and stored in 30% sucrose-formalin solution until fully submerged, and sectioned coronally at 40 μm intervals. The sections were mounted and stained with 0.1% cresyl violet, and each section was photographed. These images were used to identify tetrode tracks, on the basis of the known tetrode bundle configuration. A depth reconstruction of the tetrode track was carried out for each recording session to identify the specific areas in which the units were recorded.

Statistics. Parametric tests were used to determine statistical significance. Pearson product-moment correlations were used to test the linear relationship between variables. Paired, two-sided t-tests were used to compare information scores in the laboratory and landmark frames of reference, which assumes normality. To prevent sampling the same cells across days for this analysis, the experimental session with the greatest number of units was chosen for each rat and for each tetrode. Wilcoxon rank-sum tests were used to test differences in behavioural variables.

Code availability. Custom code was written to analyse the datasets used in this study, and to generate figures for this manuscript. This codebase is versioned, and uses several third-party packages, the license files for which are included with the respective code. Access to the codebase can be provided by the corresponding author upon reasonable request.

Reporting summary. Further information on research design is available in the Nature Research Reporting Summary linked to this paper.

Data availability

The datasets used in this study are available from the corresponding author upon reasonable request.

33. Quigley, M. et al. ROS: an open-source Robot Operating System. In *ICRA Workshop on Open Source Software* (IEEE, 2009).
34. Csicsvari, J., Hirase, H., Czurkó, A., Mamiya, A. & Buzsáki, G. Oscillatory coupling of hippocampal pyramidal cells and interneurons in the behaving rat. *J. Neurosci.* **19**, 274–287 (1999).
35. Skaggs, W. E., McNaughton, B. L., Gothard, K. M. & Markus, E. J. in *Advances in Neural Information Processing Systems 5* (eds. Hanson, S. J., Cowan, J. D. & Giles, C. L.) 1030–1037 (NIPS, 1992).
36. Zhang, K., Ginzburg, I., McNaughton, B. L. & Sejnowski, T. J. Interpreting neuronal population activity by reconstruction: unified framework with application to hippocampal place cells. *J. Neurophysiol.* **79**, 1017–1044 (1998).
37. Kloosterman, F., Layton, S. P., Chen, Z. & Wilson, M. A. Bayesian decoding using unsorted spikes in the rat hippocampus. *J. Neurophysiol.* **111**, 217–227 (2014).
38. Brown, E. N., Frank, L. M., Tang, D., Quirk, M. C. & Wilson, M. a. A statistical paradigm for neural spike train decoding applied to position prediction from ensemble firing patterns of rat hippocampal place cells. *J. Neurosci.* **18**, 7411–7425 (1998).
39. Flandrin, P., Francois, A. & Chassande-Mottin, E. in *Applications in Time-Frequency Signal Processing* (ed. Papandreou-Suppappola, A.) 179–204 (CRC Press, Boca Raton, 2002).
40. Campbell, M. G. et al. Principles governing the integration of landmark and self-motion cues in entorhinal cortical codes for navigation. *Nat. Neurosci.* **21**, 1096–1106 (2018).

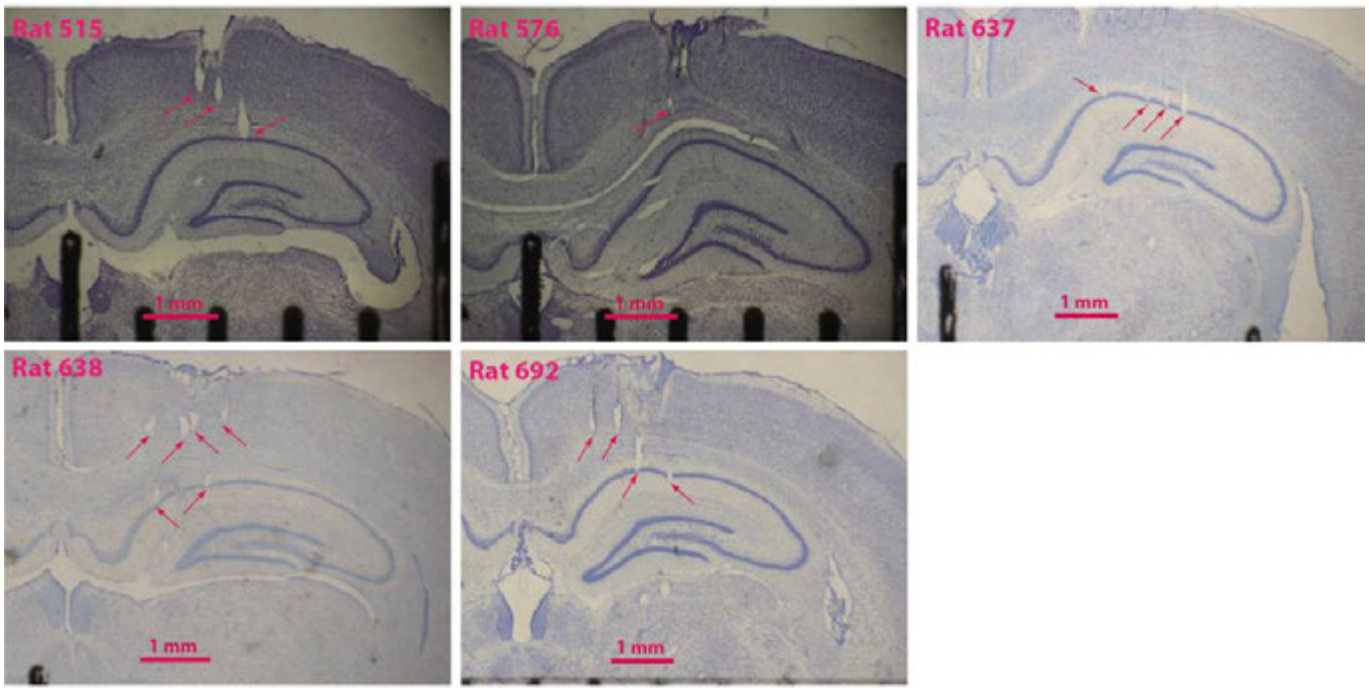

Extended Data Fig. 1 | Representative histology. Coronal slices from the five rats used in this study. Arrows point to tetrode tracks at different stages of advancement towards CA1. Note that these are not always the termination of these tetrodes, simply one section along their tracks. In one rat (576), the histology was inconclusive owing to poor fixation and slice quality; however, we determined that the tetrodes were correctly placed in CA1 by the mediolateral placement of the bundle, tracks in the few sections that we could analyse, and features in the EEG signals observed during recording (for example, sharp waves and ripples). In one rat (638), two of the most medial tetrodes (not shown) appeared to record from the fasciola cinereum, rather than CA1.

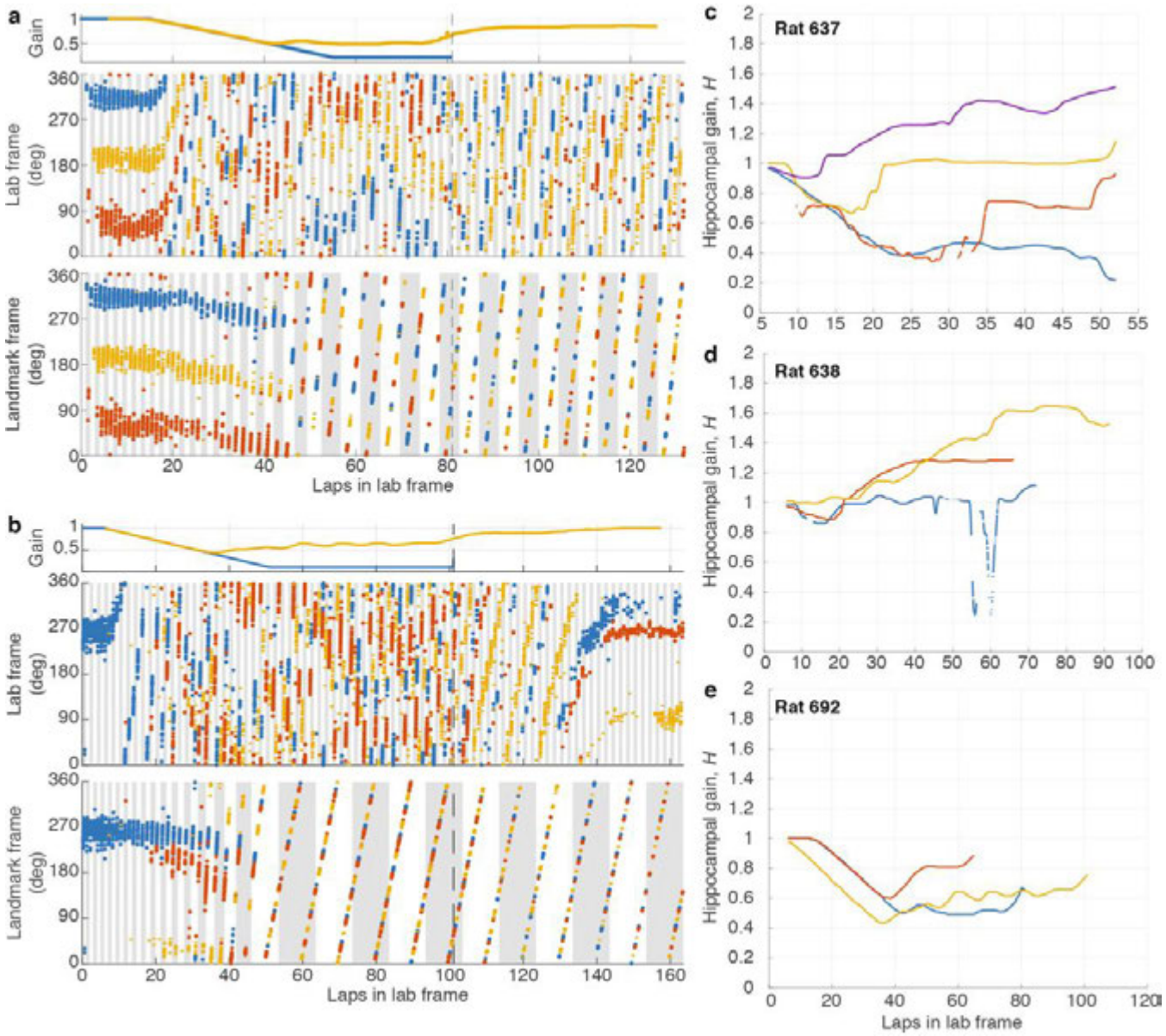

Extended Data Fig. 2 | Examples of failure of landmark control. a, Top, experimental gain, *G* (blue), and hippocampal gain, *H* (yellow), for epochs 1–3 of a session in which G_{final} was 0.231. Note that the two curves overlap until about lap 40, when they start to diverge. Middle, spikes from three putative pyramidal cells (coloured dots) in the laboratory frame. Alternate grey and white bars indicate laps in the laboratory frame. Bottom, the same spikes in the landmark frame. At the point of landmark-control failure, the place cells stop firing at a particular location in the landmark frame, and instead start drifting in both laboratory and landmark frames. Alternate grey and white bars indicate laps in the landmark frame. **b**, Second example, from a different rat, for a session in which G_{final} was 0.1 (same format as **a**). **c**–**e**, Trajectory of hippocampal gain, *H*, for three rats for all sessions in which landmark control failed. The hippocampal gain generally starts near to one, and then diverges from the experimental gain trajectory (not shown) during the session.

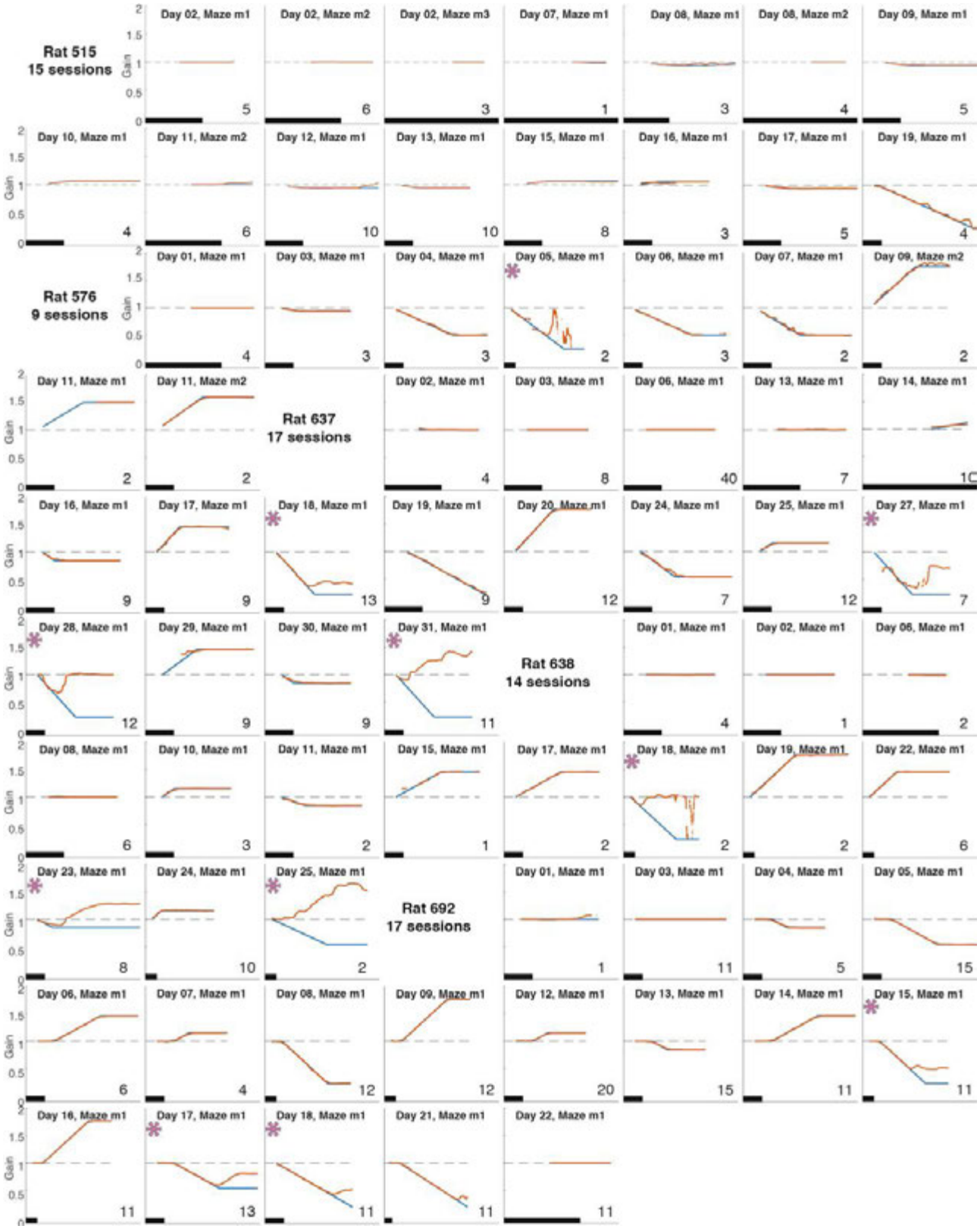

Extended Data Fig. 3 | Gain dynamics during each session. Each plot represents data from a single session during epochs 1–3 (landmarks on). The *x* axis is the laps that the rat ran in the laboratory frame (on the table) and the *y* axis is gain. The black scale bar in each plot indicates 10 laps. The applied experimental gain *G* (blue) is plotted with the hippocampal gain estimate *H* (orange). The ramp rate, length of epochs and final experimental gain for each session can be observed from the curves. Asterisks indicate sessions with loss of landmark control (mean gain ratio greater than 1.1; see Fig. 2h). In the other plots, the blue and red curves overlap, indicating control of landmarks over the place fields. The number of units that passed the acceptance criteria (Methods) in each session is indicated in the bottom right-hand corner of each plot.

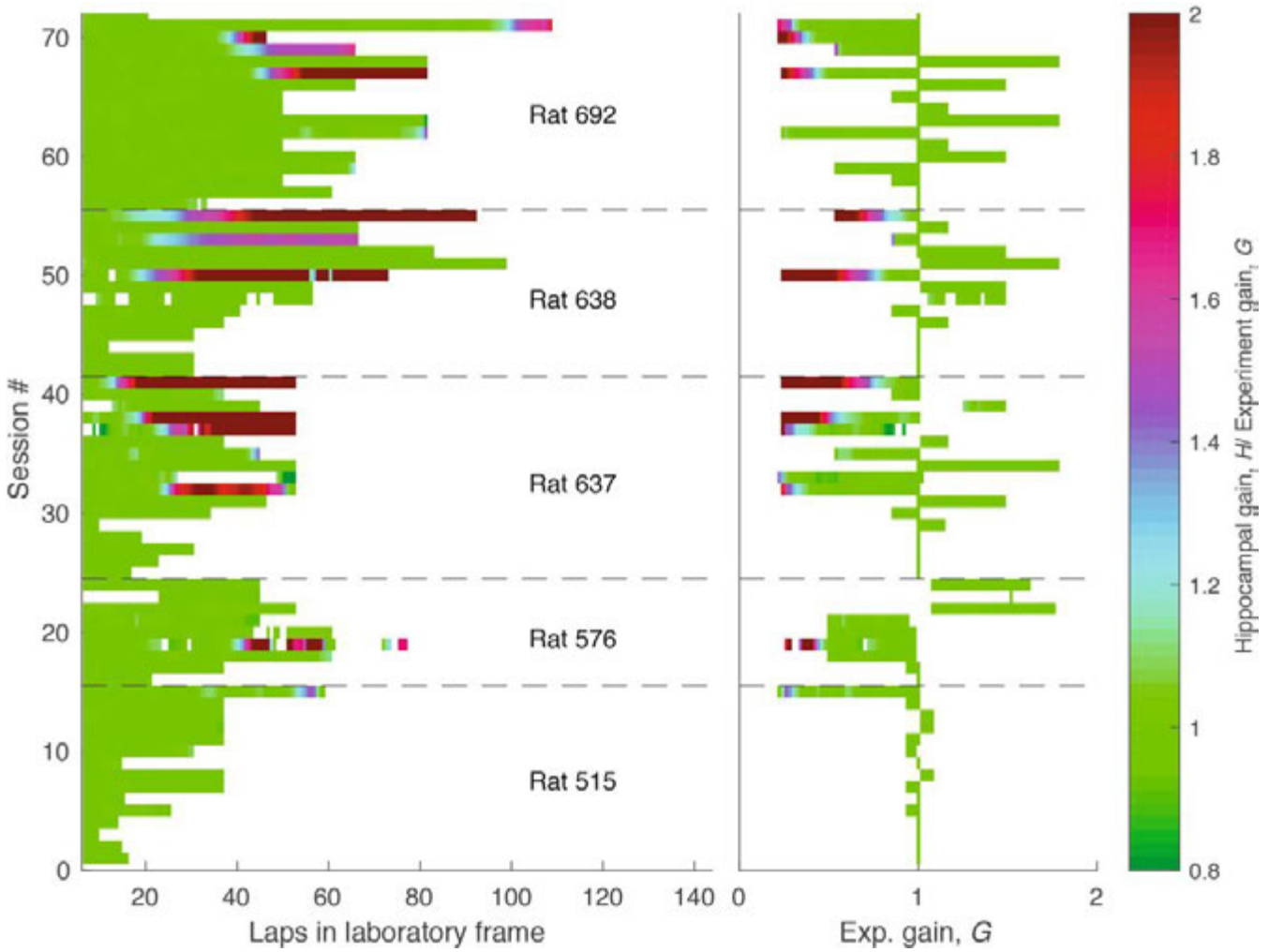

Extended Data Fig. 4 | Summary of dataset. Each row indicates 1 of the 72 sessions comprising the dataset during the period in which the landmarks were on. In the left plot, the *x* axis is laps in the laboratory frame. In the right plot, the *x* axis is the experimental gain, *G*. The sessions are chronologically ordered (bottom to top). Sessions from different rats are separated by dashed lines. In all rats, we typically performed smaller manipulations in *G* first, as initial landmark failure tended to occur at larger manipulations of *G*. Once landmark control failed, it tended to fail more frequently. The colour represents the ratio between hippocampal and experimental gains (*H*/*G*, colour bar, right). Green ($H/G = 1$) indicates landmark control. Four of the rats (576, 637, 638 and 692) experienced landmark failure (red portions of sessions). Failures happened only when *G* was less than one (that is, the landmarks moved in the same direction as the rat), and generally occurred at low values of *G* (less than 0.5) and after rats had experienced several gain-manipulation sessions over days. The asymmetry in landmark control between $G < 1$ and $G > 1$ is similar to a study of medial entorhinal cortex[40]. In that study, mice ran on a virtual-reality linear track controlled by a stationary treadmill, and the gain factor was manipulated between the distance travelled on the treadmill versus the virtual-reality track. Grid cells showed asymmetric responses to increases compared with decreases of the gain. Gain increases ($G > 1$) caused phase shifts in the spatial firing patterns, but gain decreases ($G < 1$) caused changes in the spatial scales. These results were explained by a model of how grid cells respond to conflicts between self-motion and landmark cues. Although the study did not address the issues of path-integration gain recalibration, as in our current work, its results may provide a causal explanation for the asymmetric responses of place cells to the landmark manipulations seen in the present study.

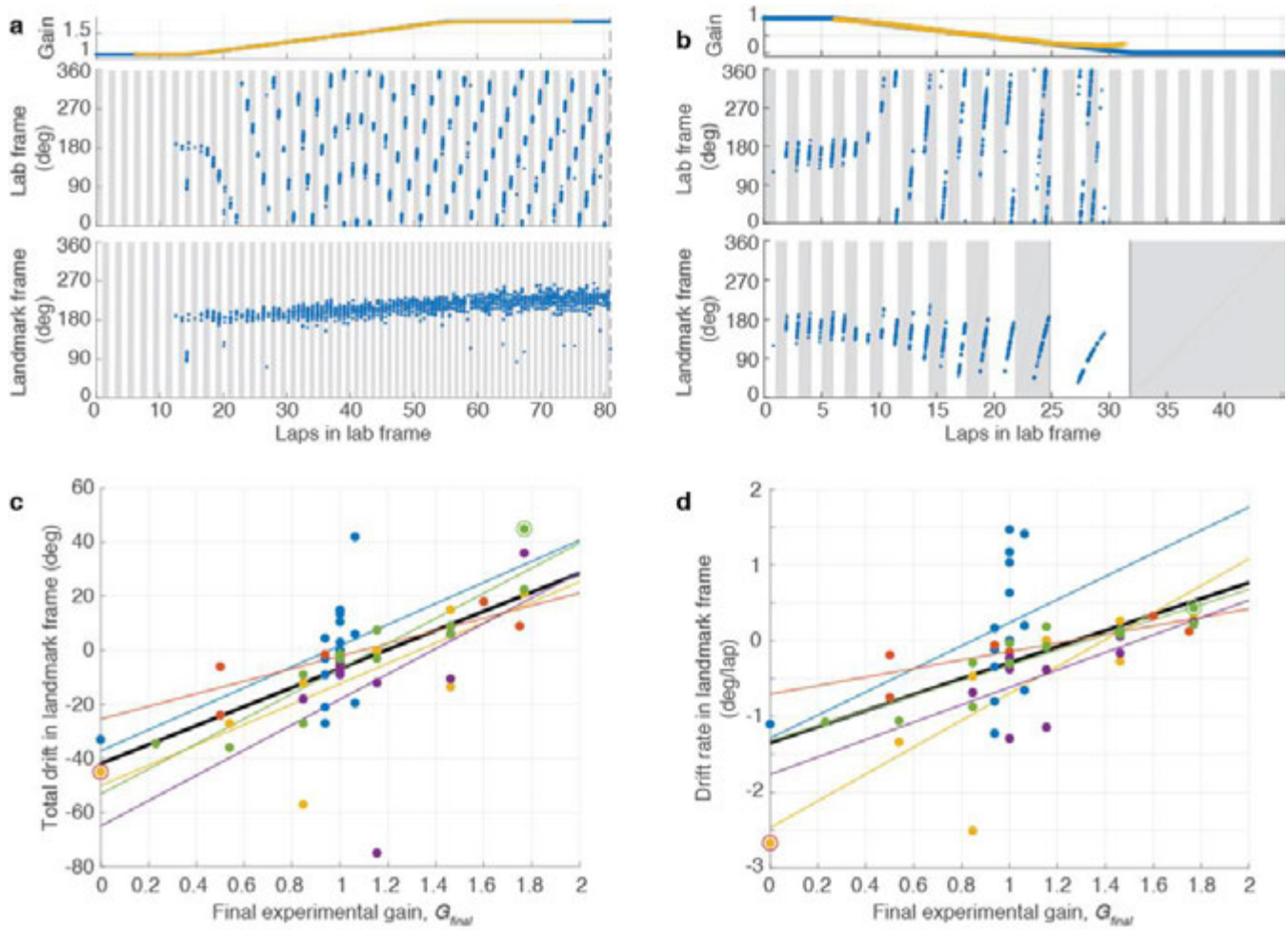

Extended Data Fig. 5 | Slow drift of place fields against landmarks. **a**, Example of positive drift. Top, experimental gain, G (blue), and hippocampal gain, H (yellow), for epochs 1–3 of a session in which G_{final} was 1.769. There is no H (yellow) in the first or last 6 laps owing to the 12-lap sliding window. Middle, spikes from one putative pyramidal cell (blue dots) in the laboratory frame. Figure format is the same as in Fig. 2. Bottom, the same spikes in the landmark frame. The unit was silent for the first 12 laps but developed a strong place field in the landmark frame, which slowly drifted in the same direction as the movement of the rat over the course of the session. **b**, Example of negative drift from a session in which G_{final} was 0. In the landmark frame, the slow drift was in the direction opposite to the direction of movement of the rat. Note that the unit was completely silent in epoch 3, because the rat was not in the place field of the unit as G reached 0. **c**, Drift over the entire session plotted against G_{final}. Each point represents an experimental session. Linear fits are shown for each individual rat (coloured lines) and for the combined data (black line; $n = 55$ sessions, Pearson's $r_{53} = 0.64$, $P = 1.5 \times 10^{-7}$). The two example sessions of **a** and **b** are marked with a circle. **d**, Drift rate against G_{final}. Although the magnitude of drift is correlated with the final experimental gain (G_{final}), as shown in **c**, a confound is present because the ramp duration in epoch 2 depends on the value of G_{final} (for example, for $G > 1$, the larger the value of G_{final}, the more laps are required to ramp G up to that value). It is thus possible that the correlation between the total drift and G_{final} is due to the differences in duration of epoch 2 (and, in some sessions, epoch 3) rather than due to different rates of drift that depend on G. To control for the effect of session duration, we calculated drift rate by dividing the total drift by the total number of laps in the landmark frame over which the drift was computed. Linear fits are shown for each individual rat (coloured lines) and for the combined data (black line; $n = 55$ sessions, Pearson's $r_{53} = 0.54$, $P = 1.9 \times 10^{-5}$). The two example sessions of **a** and **b** are marked with circles. These results show that the drift rate was related to the value of G_{final}.

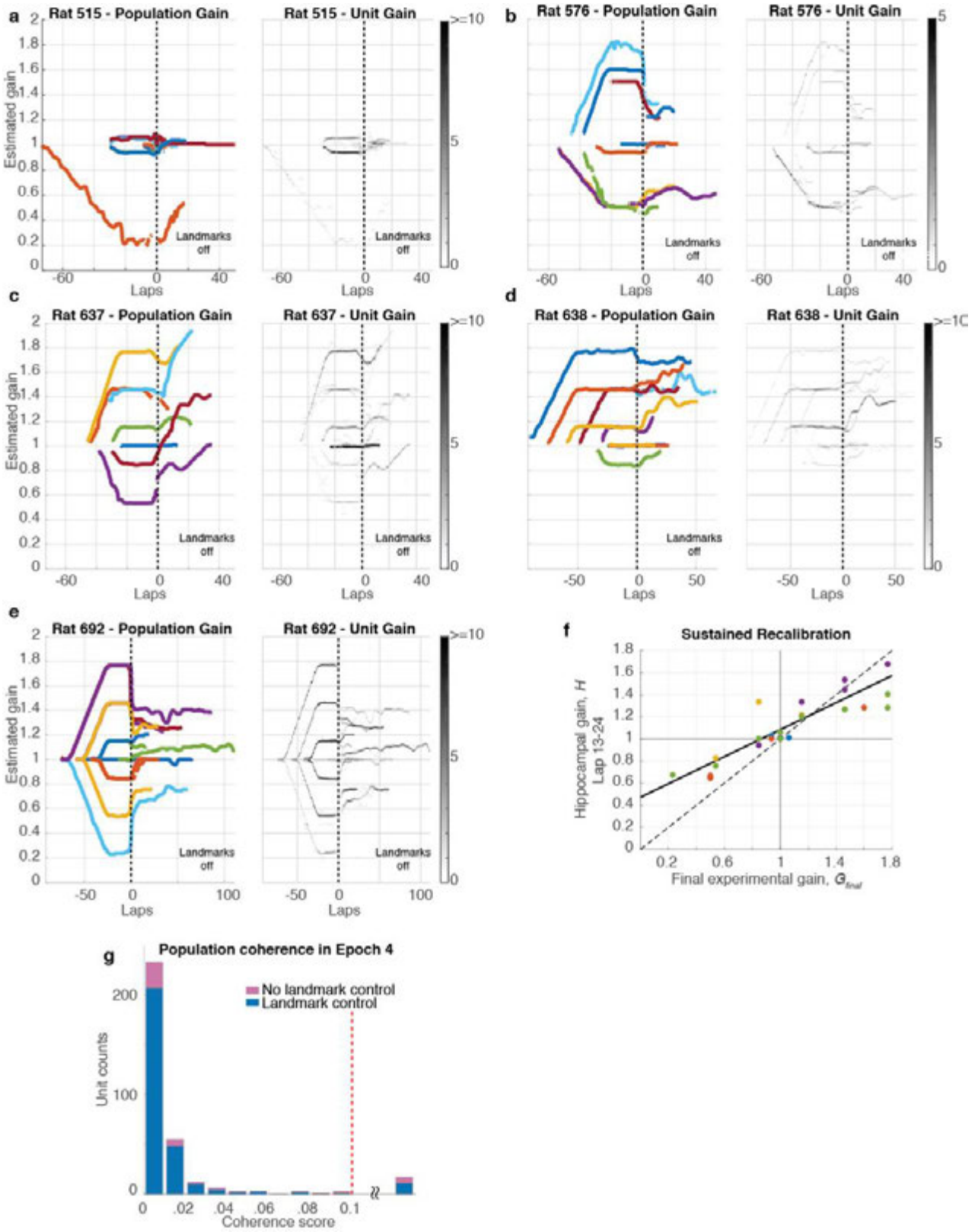

Extended Data Fig. 6 | See next page for caption.

Extended Data Fig. 6 | Dynamics of recalibration. a–e, The complete hippocampal gain (H) dynamics for all five rats for sessions that exhibited landmark control. The gain dynamics for rat 692 is also shown in the main text (Fig. 3e). In the left panels for each rat (colour), H is plotted as a function of laps run in the laboratory frame. Sessions are aligned to the instant when the landmarks were turned off (denoted as lap 0). In the presence of landmarks (before lap 0), the hippocampal gain tracked the experimental-gain profiles during a given session (not shown). After the landmarks were turned off, the traces largely maintained their recalibrated gain, while also showing some variable drift across sessions. Note that for each rat, for sessions in which $G = 1$ (that is, the landmarks did not move), the value of H was close to 1 when the landmarks were turned off. The right panels for each rat show the gain trajectories of all the units in the dataset. The grey scale represents the number of active cells with gains falling in a given bin (bin size is 5° for laps axis and 0.01 for gain axis). These graphs demonstrate the high degree of coherence of the hippocampal population, as almost all cells shared the same gain with minimal deviation. The light-coloured lines that occasionally deviate from the main trajectories arise from the small number of cells with poor spatial tuning or from cells that remapped. In the latter case, because our spectral gain analysis used a window of 12 laps, these remapped cells continued to show artefactual values for the limited number of laps that fall in this window but during which the cell was silent. As can be seen, these exceptions had negligible influence on the median population gain values. **f**, Sustained recalibration. Comparison of G_{final} (x axis) and H computed using laps 13–24 (that is, the value of H at lap 18) after the landmarks were turned off (y axis). Sessions for each rat are plotted in different colours, along with the perfect recalibration line (dashed line, black) and a linear fit (solid line, black; $n = 27$ sessions, Pearson's $r_{25} = 0.85$, $P = 2.04 \times 10^{-8}$). The number of data points is lower than in Fig. 3c because some sessions ended before lap 24. **g**, Histogram of coherence scores (same format as Fig. 2g) for units firing during epoch 4 (landmarks off). The shape of the histogram is very similar to that of Fig. 2g. Almost all units had a coherence score of less than 0.1, indicating that the place fields acted as a coherent population in sessions with (blue) and without (pink) landmark control in epochs 1–3, even after the landmarks were turned off. Units with a coherence score of greater than 0.1 (range 0.11–0.41) were combined in a single bin (17/336 units).

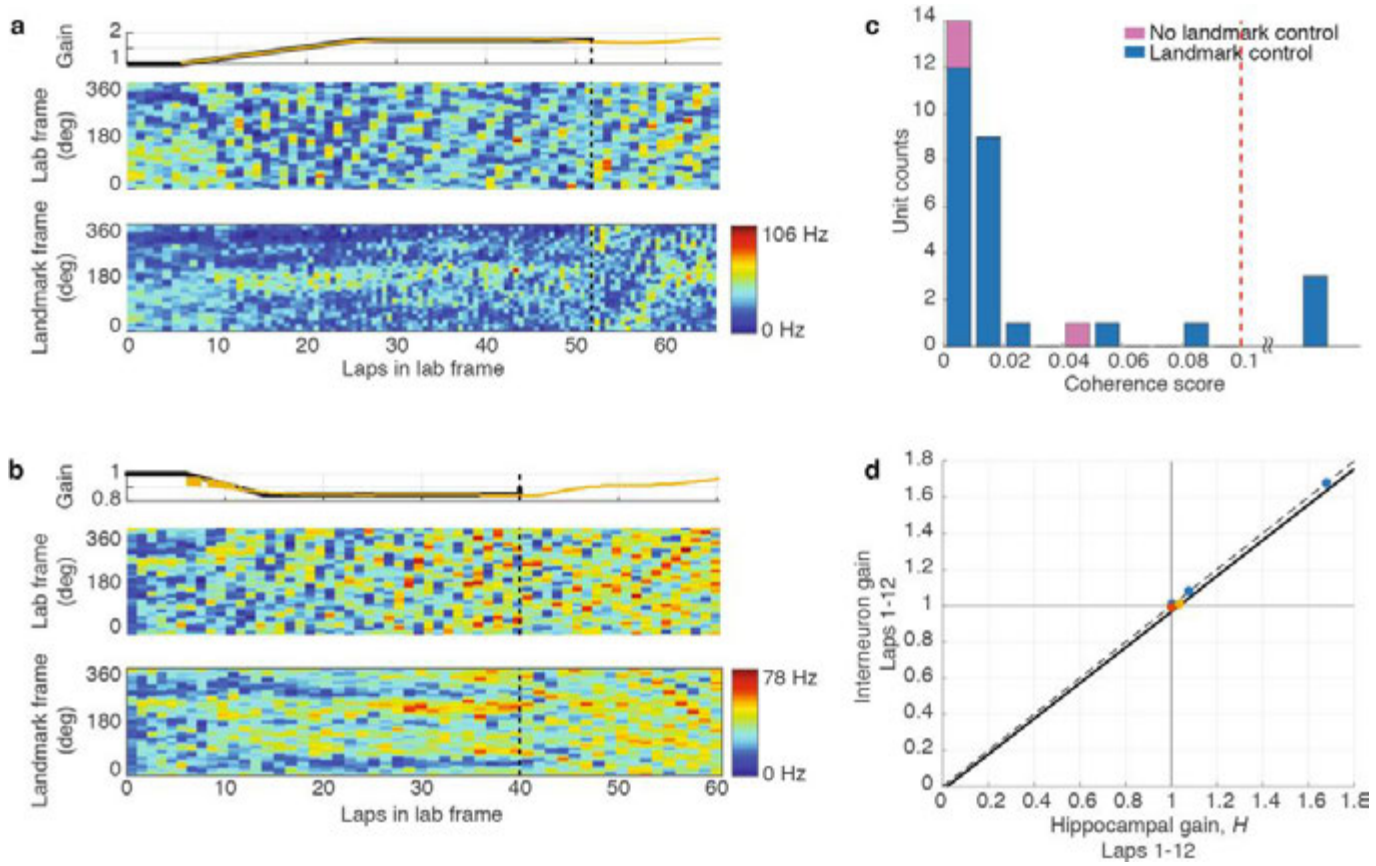

Extended Data Fig. 7 | Path-integration gain recalibration is also demonstrated by hippocampal interneurons. a, Top, experimental gain, G (black) and hippocampal gain, H (yellow) for epochs 1–4 of a session in which G_{final} was 1.769. H was computed as usual from putative pyramidal cells (see 'Estimation of hippocampal gain' in Methods). In epoch 4, landmarks are turned off, hence there is no G. Middle, spatiotemporal rate map of one putative interneuron in the laboratory frame. Owing to the high firing rate of interneurons, rate maps are more illustrative than the spike plots used in place-cell examples. Each horizontal bin represents a lap in the laboratory frame, similar to the alternating grey and white vertical bands in the place cell examples (for example, Fig. 2a, c, e). Each vertical bin spans 3° in the laboratory frame. Bottom, rate map of the same unit in the landmark frame. Each horizontal bin represents a lap in the landmark frame, and each vertical band spans 3° in the landmark frame. Note that the firing pattern is preserved across laps until epoch 4, when the landmarks turn off. **b**, Example of a putative interneuron in a session in which G_{final} was 0.846. Same format as **a**. **c**, Histogram of coherence score between interneurons and putative pyramidal cells, as in Fig. 2g. The score for each putative interneuron is computed as the mean value of $|1 - I/H|$ over the entire session, in which I is the spectral gain estimated from the interneuron and H is the hippocampal gain computed as usual from putative pyramidal cells. Units with coherence score above 0.1 (range 0.15–0.24) were combined in a single bin. **d**, H estimated using the first 12 laps after the landmarks were turned off, using the median of estimates from putative pyramidal cells compared to the median of estimates from putative interneurons. There are only five data points because these are the subset of sessions in Fig. 3c with simultaneously recorded putative interneurons and place cells.

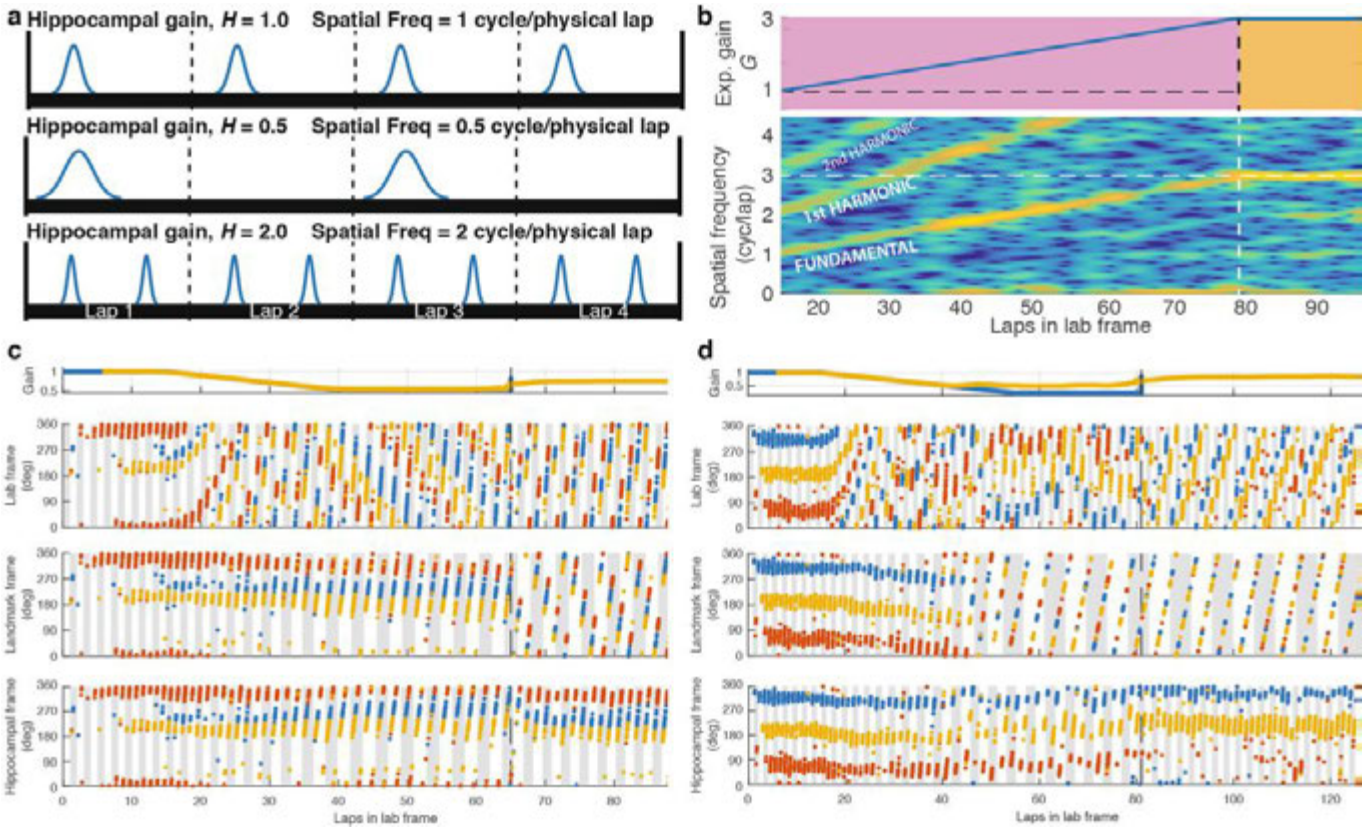

Extended Data Fig. 8 | Illustration of spectral decoding scheme. In the dome, as visual landmarks are presented and moved at an experimental gain G, the rat encounters a particular landmark every $1/G$ laps (the spatial period). If the place fields fire at the same location in the landmark reference frame, the firing rate of the cell exhibits a spatial frequency of G fields per lap. **a**, Illustration of place-field firing for three values of hippocampal gain, H. **b**, Data from a session in which G was gradually increased from 1 to 3 (top) as in epoch 2 of our sessions. The spectrogram of one unit is shown at the bottom, with the colour denoting the power at a given position and frequency. A clear set of peaks in the spectrogram emerges at spatial frequencies corresponding to the experimental gain and at its harmonics. We use a custom algorithm to trace these peaks (see 'Estimation of hippocampal gain' in Methods) and estimate the gain for each unit. The hippocampal gain, H, is estimated by taking the median spatial frequency across all isolated units (H_i for the ith unit) for a given session. Note that this method does not require that cells display single, sharply tuned place fields, as it works for cells with multiple fields as well as for interneurons (Extended Data Fig. 7). **c**, Reproduction of Fig. 3b, along with an additional panel at the bottom that represents the same spikes in the 'hippocampal frame'; that is, the spikes were plotted in the frame of the landmarks as if they were rotating at the calculated gain of the place-cell map (the hippocampal gain, H). The shaded vertical bars denote each lap in the hippocampal frame. Fields from all three units are horizontally aligned in this panel during all epochs, indicating that the spectral-decoding technique was successful and that the place fields acted as a coherent spatial representation within the hippocampal frame. **d**, Reproduction of Extended Data Fig. 2a, along with an additional panel at the bottom that represents hippocampal gain. In this dataset, it can be seen that even after 'failure' of landmark control of place fields, the fields are still coherently firing at the same hippocampal gain, which we are able to estimate using spectral decoding.

Extended Data Table 1 | Results of behavioural analyses

	Mean vel (°/sec)	Pauses/lap	Pause Duration (s)	Interpause Interval (s)	Interpause Distance (°)	G_{final}
Mean (S.E.M.)						
Epoch 1	24.6 (0.7)	0.9 (0.2)	8.8 (1.0)	55.8 (8.2)	887 (136)	--
Epoch 2	25.2 (0.9)	1.0 (0.1)	6.5 (0.5)	61.8 (18.0)	1119 (399)	--
Epoch 3	25.0 (1.0)	1.5 (0.2)	8.8 (1.0)	26.3 (3.5)	461 (79)	--
Epoch 4	24.2 (1.0)	1.5 (0.3)	9.2 (0.8)	34.9 (9.4)	531 (125)	--
Epochs 3-1	0.4 (0.5)	*0.5 (0.2)	0 (1.5)	*-29.6 (7.9)	*-426 (121)	--
Epochs 4-3	-0.8 (0.4)	0.1 (0.2)	0.3 (1.3)	8.6 (9.8)	69 (134)	--
Multiple regression						
Epoch 4 – Epoch 3						
β	-0.01	0	0	0	0	0.65
S.E.	0.01	0.02	0	0	0	0.05
Epoch 3 – Epoch 1						
β	0.01	-0.01	0.01	0	0	0.66
S.E.	0.01	0.03	0	0	0	0.05

Two-sided Wilcoxon signed-rank tests were performed on the differences between values in epochs 3 and 1 and epochs 4 and 3 with the null hypothesis that the difference = 0. Pauses/lap ($n = 37$ sessions; $P = 0.035$); interpause interval ($n = 37$ sessions; $P = 0.001$); interpause distance ($n = 37$ sessions; $P = 0.003$). All other tests for epochs 3–1 and epochs 4–3 were not significant.

nature research

Corresponding author(s): James Knierim

Reporting Summary

Nature Research wishes to improve the reproducibility of the work that we publish. This form provides structure for consistency and transparency in reporting. For further information on Nature Research policies, see Authors & Referees and the Editorial Policy Checklist.

Statistical parameters

When statistical analyses are reported, confirm that the following items are present in the relevant location (e.g. figure legend, table legend, main text, or Methods section).

n/a	Confirmed	
☐	☒	The exact sample size (*n*) for each experimental group/condition, given as a discrete number and unit of measurement
☐	☒	An indication of whether measurements were taken from distinct samples or whether the same sample was measured repeatedly
☐	☒	The statistical test(s) used AND whether they are one- or two-sided *Only common tests should be described solely by name; describe more complex techniques in the Methods section.*
☒	☐	A description of all covariates tested
☐	☒	A description of any assumptions or corrections, such as tests of normality and adjustment for multiple comparisons
☐	☒	A full description of the statistics including central tendency (e.g. means) or other basic estimates (e.g. regression coefficient) AND variation (e.g. standard deviation) or associated estimates of uncertainty (e.g. confidence intervals)
☐	☒	For null hypothesis testing, the test statistic (e.g. *F*, *t*, *r*) with confidence intervals, effect sizes, degrees of freedom and *P* value noted *Give P values as exact values whenever suitable.*
☒	☐	For Bayesian analysis, information on the choice of priors and Markov chain Monte Carlo settings
☒	☐	For hierarchical and complex designs, identification of the appropriate level for tests and full reporting of outcomes
☐	☒	Estimates of effect sizes (e.g. Cohen's *d*, Pearson's *r*), indicating how they were calculated
☐	☒	Clearly defined error bars *State explicitly what error bars represent (e.g. SD, SE, CI)*

Our web collection on statistics for biologists may be useful.

Software and code

Policy information about availability of computer code

Data collection	Windows Operating System version 8.1; Ubuntu Linux Operating System versions 12.04, 14.04; Neuralynx Cheetah V5; Robot Operating System (ROS) versions Hydro, Indigo; Xenomai Real-Time Framework versions 2.6, 3.0.
Data analysis	MATLAB versions 2017a, 2017b, 2018a; Various open-source third-party MATLAB packages from mathworks.org; custom WinClust software for spike sorting (written by J. Knierim)

For manuscripts utilizing custom algorithms or software that are central to the research but not yet described in published literature, software must be made available to editors/reviewers upon request. We strongly encourage code deposition in a community repository (e.g. GitHub). See the Nature Research guidelines for submitting code & software for further information.

Data

Policy information about availability of data

All manuscripts must include a data availability statement. This statement should provide the following information, where applicable:

- Accession codes, unique identifiers, or web links for publicly available datasets
- A list of figures that have associated raw data
- A description of any restrictions on data availability

The datasets used in this study are available from the corresponding author upon reasonable request.

Field-specific reporting

Please select the best fit for your research. If you are not sure, read the appropriate sections before making your selection.

☒ Life sciences ☐ Behavioural & social sciences ☐ Ecological, evolutionary & environmental sciences

For a reference copy of the document with all sections, see nature.com/authors/policies/ReportingSummary-flat.pdf

Life sciences study design

All studies must disclose on these points even when the disclosure is negative.

Sample size	No statistical methods were used to pre-determine sample size in these exploratory studies. The number of animals was determined based on standards used to established results in other peer-reviewed publications in the field. The number of sessions per animal varied based on behavioral state, number of units being recorded and observed stability of recordings. The main effects seen in this study were demonstrated in all 5 animals, indicating that the effects are robust and reliable.
Data exclusions	Sessions were excluded from analysis if they did not meet all of the following criteria. Criteria 1-4 are standard for our lab and were pre-established. Criteria 5-6 were specific for this experiment, not pre-established but were used to ensure that the session provided data of sufficient quality to address the experimental question. None of the exclusion criteria affected or biased the experimental results. (1) There were no experimental disruptions, such as too much manual intervention during the session or too many long breaks in recording due to behavioral performance or technical issues. (2) At least one unit deemed 'fair' or above, according to our manual quantification of cluster isolation quality. (3) At least one unit having more than 50 spikes during the session that fired when the animal ran at a velocity of more than 5 cm/s. (4) At least one unit classified as a putative pyramidal cell, using our classification based on mean firing rate, spike width, and typical ISI. (5). The rat ran at least 12 laps in the session with landmarks on. (6) Our population decoding method was able to provide a population hippocampal gain estimate for at least half of the duration while the landmarks were on.
Replication	We performed the experiment independently on five different individual rats. All rats showed the main findings. There have been no indications that would prevent replication of these results, except the emergence of failure of control of the hippocampal place fields by landmarks. Since this happens upon repeated exposure to moving landmark cues, care must be taken to avoid excessive / abrupt landmark manipulation while replicating these results.
Randomization	There were no experimental groups for the subjects, since we ran similar sessions on all 5 animals used in this study.
Blinding	The investigators were not blind to the identity of the animal or the experimental gain being applied during data collection. Isolation and classification of clusters, however, was done blind to the experimental manipulation being applied. The data analysis software was also blind to the parameters of the trial.

Reporting for specific materials, systems and methods

Materials & experimental systems

n/a	Involved in the study
☒	☐ Unique biological materials
☒	☐ Antibodies
☒	☐ Eukaryotic cell lines
☒	☐ Palaeontology
☐	☒ Animals and other organisms
☒	☐ Human research participants

Methods

n/a	Involved in the study
☒	☐ ChIP-seq
☒	☐ Flow cytometry
☒	☐ MRI-based neuroimaging

Animals and other organisms

Policy information about studies involving animals; ARRIVE guidelines recommended for reporting animal research

Laboratory animals	Rattus norvegicus, Long Evans, Male, 5-8 months old, 300-450 g. weight
Wild animals	Wild animals were not involved in this study
Field-collected samples	The study did not involve samples collected from the field.